Heliyon 10 (2024) e29552

Contents lists available at ScienceDirect

Heliyon

journal homepage: www.cell.com/heliyon

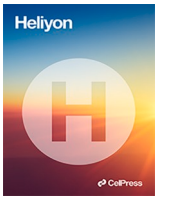

Research article

The influence of 3D-printed PLA coatings on pure and fretting fatigue properties of AM60 magnesium alloys under cyclic bending loads

Saeid Rezanezhad, Mohammad Azadi *

Faculty of Mechanical Engineering, Semnan University, Semnan, Iran

ARTICLE INFO

Keywords:
AM60 magnesium alloy
High-cycle fatigue
Fretting fatigue
3D-print
Fractography

ABSTRACT

A study was conducted to compare the pure fatigue and fretting fatigue properties of AM60 magnesium alloys, with and without 3D-printed PLA coatings. The PLA coating layers led to an increase in the fatigue lifetime in both pure and fretting conditions. They delayed the crack initiation time compared to uncoated samples, thereby increasing fatigue lifetime. Additionally, in the case of fretting fatigue, PLA coating caused the fretting pads to reach the magnesium alloy later, which also contributed to the longer lifetime of coated samples, compared to uncoated specimens. Using field emission scanning electron microscopy, all specimens exhibited the brittle fracture behavior, with the presence of both cleavage and quasi-cleavage marks. By the fractography, it was found that the number of cracks in coated samples decreased in both pure and fretting fatigue conditions. Remarkably, PLA coating during fretting fatigue resulted in a significant enhancement of the fretting fatigue lifetime, within 56%–2182 %.

1. Introduction

One of the key areas of mechanics is the classification of mechanical failure processes in structures. One of the most intricate failure mechanisms that result from the interaction of wear and fatigue is fretting fatigue. The fretting phenomenon refers to the relative tangential movement between two objects in contact when subjected to vibration loads or changing forces [1–3]. In certain parts, the process of fretting fatigue damage is regarded as substantial harm, and even though this subject has been researched for over a century, more research is still needed to understand the behavior and principles of fretting fatigue mechanisms [4,5].

The usage of magnesium alloys in numerous components has increased in recent decades due to their unique mechanical properties; among these parts are vehicle parts and implants used in the human body [6,7]. Magnesium has a density and Young modulus that are similar to bone, unlike commonly used metallic implants [8,9], This similarity may help to reduce stress-shielding effects. A significant factor is that there is no need for a subsequent surgical procedure to eliminate the metal bone plates as magnesium can be gradually dissolved, assimilated, metabolized, or expelled [10].

Magnesium alloys have limited potential for future use because they deteriorate quickly in the body and fluids, and if left untreated, they cannot maintain their mechanical performance until the tissue has sufficiently healed [11]. Surface modification methods such as electrochemical deposition [12], conversion coatings [13], laser surface alloying [14], alkaline treatment [15], micro-arc oxidation [16,17], and sol-gel coatings [18] have all been proposed. Another type of coating that has been used on magnesium alloys is PLA

* Corresponding author.
E-mail address: m_azadi@semnan.ac.ir (M. Azadi).

https://doi.org/10.1016/j.heliyon.2024.e29552
Received 14 December 2023; Received in revised form 23 March 2024; Accepted 10 April 2024
Available online 16 April 2024

coating on this alloy, which some researchers [6,19,20] have used in their research. Several biodegradable polymers, including Polycaprolactone (PCL), Polylactic glycolic acid (PGA), and Polylactic acid (PLA) have been approved for utilization in clinical settings for humans. These polymers are utilized in small load-bearing bone implants and cardiovascular therapies [21]. Biodegradable polymers, on the other hand, can provide corrosion protection as well as additional capabilities such as medication transport and the capacity to be functionalized with organic biomolecules [22].

Magnesium alloys are also widely used in the transportation industry, particularly in cars and trucks, due to their advantages in lightweight design, which can significantly improve fuel efficiency and reduce vehicle emissions. However, in magnesium alloys, high sensitivity to corrosive environments limits their use in automotive applications. One of the most efficient and cost-effective strategies to prevent corrosion in magnesium alloys is surface coating [7]. One of the commonly used magnesium alloys in various industries is AM60 [23,24]. The sentences that follow provide an overview of the literature on mechanical characteristics, fretting fatigue, and fatigue of magnesium alloys.

Chen et al. [25] conducted a study on the formation of small fatigue cracks in a magnesium alloy (AM60) and examined the impact of thermomechanical processing and subsequent heat treatment on its behavior. The study analyzed the impact of stress intensity factors on the growth rates of cracks in materials with different microstructures and yield stresses, subjected to varying processing conditions. Fracture surface analysis suggests that the mechanism of fatigue crack propagation may have included transgranular and intergranular cracking. It was essential to understand the importance of porosity and other material flaws in influencing the behavior of fatigue crack initiation and propagation. Further research revealed that the large casting pores in cast magnesium alloys were the most likely locations for crack initiation [26,27], whereas wrought magnesium alloys showed both subsurface and surface fatigue crack initiations [28]. It was discovered that the stress intensity component was connected to the fatigue crack growth process. For cast magnesium alloys, fatigue fractures spread primarily through dendrite cells at low-stress intensity factors and across interdendritic zones at high-stress intensity factors [26,29]. Others have demonstrated that the beginning and spread of fatigue cracks were significantly accelerated by the sample exposure to water vapor [27,30]. The behavior of fatigue crack propagation for cracks in the physically microscopic fracture regime under diverse processing and mechanical loading circumstances has not yet been fully described.

Sadeler and Atasoy [31] conducted a study to investigate the effect of contact pad hardness on the fretting fatigue performance of AZ61 magnesium alloy. Vickers hardness levels 83.3 and 55.3 for the contact material were prepared. The study revealed that there was a decrease in the strength of fretting fatigue as the hardness increased. The tangential amplitude did not change with varying hardness, but there was an increase in the relative slip amplitude as the hardness level went up. It is believed that when hardness increases, the local tangential stress at the contact end increases, which in turn lowers the fretting fatigue strength. Magnesium alloys as a biodegradable material had their electrochemical properties thoroughly evaluated by Olugbade et al. [32]. Numerous studies have been conducted regarding the corrosion processes and corrosion fatigue in magnesium alloys that have undergone surface modification. In their study of the magnesium alloy AM50A, Pirvulescu et al. [33] discovered that the material fatigue lifetime was affected by the size of the test piece, as larger pieces resulted in a greater volume of flaws. Eisenmeier et al. [34] conducted a study on the cyclic behavior of the magnesium alloy AZ91 at 25 °C and 130 °C. Their fatigue test results showed a strong correlation with both the Manson-Coffin and Basquin models. It has been demonstrated that the surface holes serve as the origin of the cracks. Li et al. [35] conducted a study on how the fatigue behavior of the AZ61 magnesium alloy is affected by the amplitude of strain. Their findings demonstrated that the shear crack will be considerable if the strain range is more than 0.5 %. Fewer cracks will be seen when the strain range is less than 0.5 %, though. Magnesium alloys AZ91 and AM60 were the subjects of research by Rettberg et al. [36] into the low-cycle fatigue behavior and the impact of heat treatment.

According to the findings, AM60 alloy has a greater fatigue lifetime at larger strain amplitudes because of its better ductility. Magnesium alloy is used both in implants used in the human body and in most industries, including automobile manufacturing.

Most researchers have investigated the improvement of its corrosion properties with surface treatment methods, but in this article, the effect of PLA coating (PLA printed by Fused Deposition Modeling 3D printer) on AM 60 magnesium alloy and its effect on pure fatigue and fretting fatigue has been investigated. The sample fracture behaviors were analyzed through the utilization of field emission scanning electron microscopy (FESEM). It is worth mentioning that the adhesion test of PLA on magnesium alloy has been studied in previous research [37]. The adhesion strength of PLA printed on AM60 magnesium alloy was measured by the epoxy glue, 4.29 ± 0.71 MPa.

2. Materials and experiments

The aim of this study was to examine the fatigue characteristics of the AM60 alloy, specifically focusing on fretting fatigue and pure fatigue. Additionally, the potential influence of a PLA coating was taken into account. It was determined that the alloy consisted of 5.90 % aluminum by weight, 0.37 % manganese by weight, 0.11 % zinc by weight, and the remaining composition was magnesium. This composition was compared to that of the AM60A alloy specified in the ASTM-B94 standard [23,24].

The PLA coating was applied using an additive manufacturing 3D printer under specific conditions. The FDM (fused deposition modeling) 3D printer creates an object by utilizing a computer to deposit molten material in a predetermined path, layer by layer. This type of printer utilizes filaments made of polymers as its raw materials. To improve the print quality, the nozzle temperature of the device was adjusted to 245 °C and the bed temperature was set to 60 °C. The samples had a density of 100 % in their initial and final layers, while the inner part had a density of 50 % with a square pattern. The device perimeter speed was set to 50 mm/s, while the infilling speed inside the part was 60 mm/s. These parameters were chosen based on the information available in the literature [38]. The nozzle diameter used was 0.4 mm, and each layer was 50 μm thick. It is worth mentioning that in the end, the thickness of the

applied PLA layer was 0.4 mm. The microstructure of a material directly influences its strength. Therefore, investigating the microstructure of the fractured surface is crucial to understanding the fracture behavior and failure mode [39]. In a parallel study [37] with this research, the fractured interface of the tensile samples was analyzed after the tensile test. Also, the mechanical properties of PLA have been discussed and examined in detail in that research. It is worth mentioning that the microstructure of PLA coating is shown in Fig. 1.

To conduct the pure fatigue tests, the Santam Company (SFT-600) was utilized along with a two-point completely reversed rotary bending loading test apparatus with $R_\sigma = -1$. The ISO-1143 standard was used as a reference for testing. A load frequency of 6000 rpm (100 Hz) was used, similar to the power rating of a car engine [40,41]. The maximum limit for fatigue lifetime testing was set at one million loading cycles [42]. Experimental reproducibility was also checked by testing at least three fatigue samples for each stress level. To establish the S–N curve, fatigue tests were carried out at five different stress levels ranging from around 60 MPa–140 MPa, plotting the stress amplitude against the fatigue lifetime. Fig. 2 displays the actual image of the standard sample along with its geometry, with and without PLA coating.

A fretting module was designed and produced for the purpose of conducting fretting fatigue tests. This module allows fretting fatigue conditions to be applied to the standard specimen. The force bar was attached to the pads in the fretting module. The module was then further secured with two screws on the fatigue device. Fig. 3 displays the fretting module installed in the fatigue testing machine, along with the geometry of the fretting pad. This study used fretting This study employed fretting pads made of ductile cast iron piston rings to replicate a fretting loading scenario on the piston alloy. The overall geometry of the fretting module, contact type, and fretting fatigue loading align with the research [43]. To prepare for the fretting fatigue test, a device based on sampling from the ASTM 2789-10 standard and other references [43–45] was devised and manufactured [46], which enables the application of fretting contact force to the sample. In this module, the fretting pads are linked to the force rod, which applies force to the test sample via a spring. The force delivered to the test sample in this study is 10 N, which is obtained based on the force applied to the piston ring [47,48]. The samples were subjected to fractography examination using FESEM.

3. Results and discussion

3.1. Pure and fretting fatigue lifetime with and without PLA

The figures of the microstructure and XRD pattern, as well as the discussion of its results, were discussed in detail in the previous study [49], but it should be noted briefly that, in addition to the Mg element, the microstructure contained an intermetallic phase composed of Al–Mn (Al_6Mn) and Mg–Al ($Mg_{17}Al_{12}$).

In the bending fatigue machine, stress is applied to the standard test sample by placing weights with particular values in the embedding spots. The fatigue device manufacturer was given users instructions on how to compute and convert the applied weight (N) to tension (Pa), using the equation $\sigma = \frac{Mc}{I}$. A simulation in the Abaqus program revealed that this instruction is precise enough for uncoated samples. Because the thickness of the PLA coating is insignificant in comparison to the AM60 magnesium alloy sample, and PLA has much weaker mechanical properties than the AM60 magnesium alloy, the thickness of the coating can be ignored when calculating stress for the coated samples; this assumption was confirmed by simulation in Abaqus software. In this approach, the sample with cover (taking into account the thickness of the cover) was simulated in Abaqus software and loaded. Table 1 shows the stress values derived using the $\sigma = \frac{Mc}{I}$ formula in the center of the conventional fatigue test sample, as well as the stress produced from the simulation for the samples with and without coatings.

Fig. 4 depicts mesh sensitivity graphs for uncoated and coated samples. According to Figs. 4 and 0.5 is an appropriate mesh size. It is worth noting that the element types were standard, 3D, and linear, and the mesh type was hex.

Furthermore, surface-to-surface interaction and a sleeve-master connection were employed to form a PLA coating on the AM60 magnesium alloy sample. Other researchers [50] have also employed surface-to-surface interaction in Abaqus software to achieve adhesive bonding of polymer to metal. Other researchers [51,52] have employed surface-to-surface interaction to form adhesive bonds.

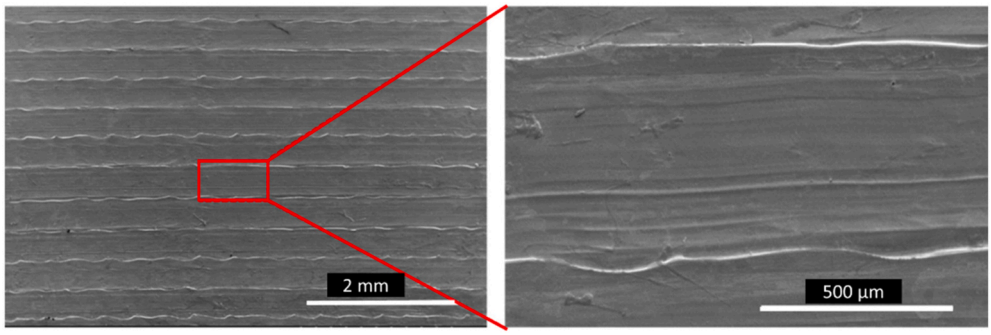

Fig. 1. The microstructure of PLA coating.

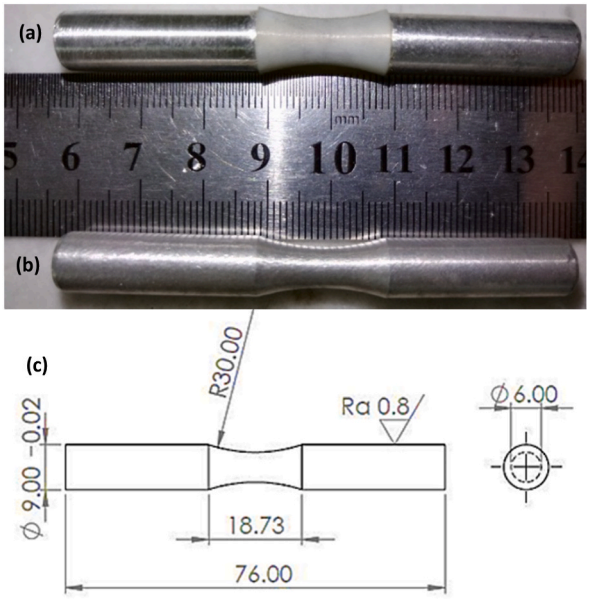

Fig. 2. The Sample for fretting fatigue and pure fatigue testing (a): with PLA, (b): without PLA, and (c): the geometry.

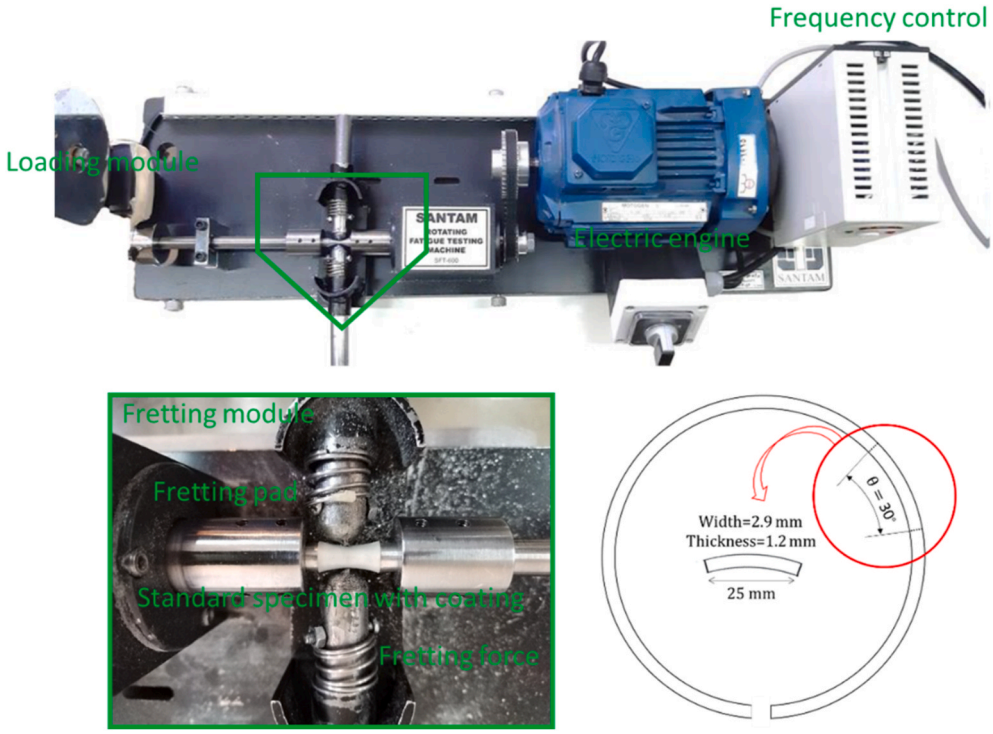

Fig. 3. The machine of rotary bending fatigue testing with the fretting module and geometry of the fretting pad.

Fig. 5 depicts the stress-lifetime (S–N) diagram of standard fatigue test samples with and without coating under pure fatigue conditions (PF). In this diagram, the stress applied to the middle of the test sample with and without coating was calculated once using the fatigue device instructions (without considering the thickness of the coating) and then, simulated again in Abaqus software, taking the coating thickness into account. Fig. 5 shows that the coating thickness can be ignored when calculating the stress applied to the sample. Figs. 6 and 7 provide an example of stress calculation using simulation in Abaqus; both stress calculations result in stress levels of 80 MPa for uncoated and PLA-coated materials, respectively. Fig. 6 (containing the uncoated sample) shows the stress level

Table 1
Stress values calculated according to the instructions of the manufacturer of the fatigue device and simulated with Abaqus.

The stress, calculated in the middle of the test sample without PLA coating with ($\sigma = \frac{mc}{i}$) formula (MPa)	Calculated stress, in the middle of the test sample without PLA coating by simulation (MPa)	Calculated stress in the middle of the test sample with PLA coating by simulation in Abaqus (MPa)	The difference percentage of the stress, calculated with the ($\sigma = \frac{mc}{I}$) formula and simulation for the uncoated sample (%)	The difference percentage of the stress, calculated with the ($\sigma = \frac{mc}{I}$) formula for the uncoated sample and the stress value obtained from the simulation for the sample with PLA coating (%)
80.40	80.32	78.97	0.09	1.70
100.20	100.00	98.39	0.19	1.80
120.40	118.30	116.30	1.70	3.30
140.40	137.20	135.00	2.20	3.80

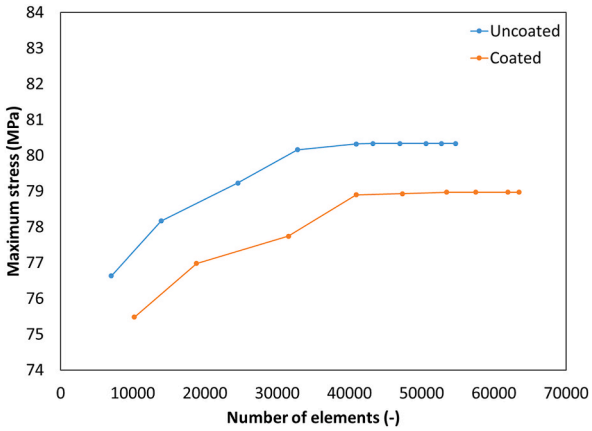

Fig. 4. Mesh sensitivity graphs for uncoated and coated sample.

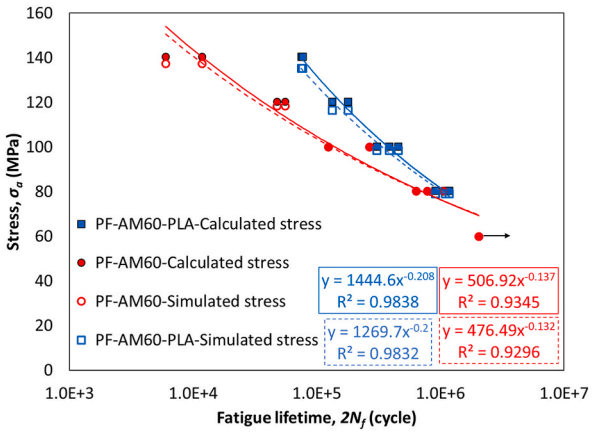

Fig. 5. The S–N diagram of the standard fatigue test samples with and without coating, under pure fatigue conditions (PF), calculated and simulated.

estimated using an Abaqus simulation. This stress level is shown in Fig. 5 with hollow circles at the stress level of 80 MPa, but due to the close proximity of the stress level, it was calculated with the simulation and the stress level calculated by the $\sigma = \frac{Mc}{I}$ formula (at the stress level of 80 MPa), the two points of the filled and empty red color almost coincide with each other. Fig. 7 also depicts the results of determining the 80 MPa stress level of PLA-coated samples using simulation in the Abaqus software. This stress level is depicted in Fig. 5 by blue empty squares. The elastic modulus for both materials was determined using a tensile test, and the Poisson coefficients for AM60 alloy and printed PLA were chosen from Refs. [53,54], respectively. These mechanical parameters are reported in Table 2.

According to the explanation, the thickness of the PLA coating will no longer be considered when calculating stress. Fig. 8 compares the stress-lifetime (S–N) curves of AM60 magnesium alloy with and without PLA coating under fretting fatigue (FF) and pure fatigue

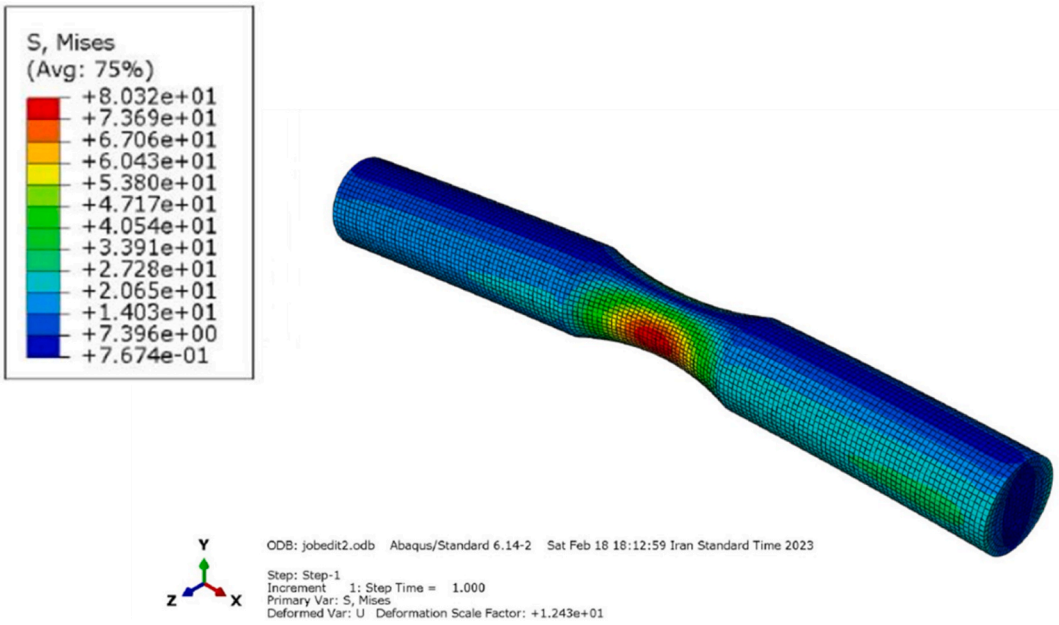

Fig. 6. Stress simulation in Abaqus software for uncoated sample.

(PF) conditions. The data is given in five different ways: (a) for all data; (b) for average data of PF-AM60 and FF-AM60; (c) for average data of PF-AM60 and PF-AM60-PLA; (d) for average data of PF-AM60 and FF-AM60-PLA; and (e) for average data of PF-AM60-PLA and FF-AM60. It is crucial to note that the results of the pure fatigue condition (without PLA) were similar to those of Chen et al. [25].

According to the findings shown in Fig. 8(a), both with and without PLA coating, the fretting fatigue condition resulted in a lower fatigue lifetime than the pure fatigue condition. The PLA-coated samples outlasted the uncoated ones in both fretting and pure fatigue situations. Fig. 8(b)–8(e) provide further information. For comparison, stress values of 120 and 80 MPa were chosen as the greatest and lowest, respectively.

Under fretting fatigue conditions, the fatigue lifetime without PLA was shown to decrease by 44.8 % and 91 % at the low-cycle fatigue regime (120 MPa) and high-cycle fatigue regime (80 MPa), respectively, as compared to the pure fatigue condition without PLA, as shown in Fig. 8(b). According to a study done by Peng et al. [55], the combination of cyclical bending stress and local contact stress may be more beneficial for the initiation and propagation of micro-cracks than simple bending fatigue. As a result, the fatigue limit and lifetime have decreased. As bending stress increases, the difference in lifetime between pure fatigue and fretting fatigue gradually diminishes. The bending stress approaches the material yield stress, resulting in this consequence. Local plastic deformation and stress concentration in microstructures promote micro-crack initiation and propagation, which reduces the impact of fretting. At stress levels of 120 MPa and 80 MPa, the fatigue lifetime under pure fatigue conditions with PLA increased by 205 % and 1183.7 %, respectively, when compared to pure fatigue conditions without PLA, as shown in Fig. 8(c). Fig. 8(d) shows that under fretting fatigue conditions, the fatigue lifetime increased by 26.0 % at the highest stress level of 120 MPa and decreased by 85.8 % at the lowest stress level of 80 MPa, compared to the pure fatigue condition without PLA.

The results depicted in Fig. 8(e) indicate that when subjected to fretting fatigue conditions, the fatigue lifetime of PLA decreased by 58.6 % and 88.9 % at the highest stress level (120 MPa) and the lowest stress level (80 MPa), respectively, as compared to pure fatigue conditions with PLA. Fig. 8(b) indicates that the reduction in fretting fatigue lifetime compared to pure fatigue lifetime (without PLA) was greater in the high-cycle fatigue range (at the lowest stress level) than in the low-cycle fatigue range (at the highest stress level). Additionally, Fig. 8(c) reveals that the addition of the coating resulted in a greater increase in pure fatigue lifetime at higher stress levels (low-cycle mode) than at lower stress levels (high-cycle mode).

It is also important that both the coated and uncoated samples exhibited an epsilon-shaped graph in the fretting fatigue tests. Notably, other researchers in previous studies have observed the epsilon-shaped behavior seen in the S–N curve of aluminum alloys under bending fretting fatigue loading. Fig. 8 shows the unusual shape of the fretting fatigue S–N diagram. Specifically, Peng et al. [55] and Parast and Azadi [56] found that the S–N curve of aluminum alloys subjected to bending fretting fatigue loading exhibited an epsilon-shaped behavior. The study concluded that increasing stress levels generally led to a decrease in fretting fatigue lifetime, except when stress levels were below 120 MPa, where an increase in stress levels improved fretting fatigue lifetime. Previous research by Peng et al. [55,57,58] has also noted three forms of fretting fatigue under bending loads, similar to the findings of this study.

The stress level can cause the groups to divide into three regimes: the slip regime (SR), the mixed fretting regime (MFR), and the partial slip regime (PSR). The different regimes are illustrated as "Stage 1," "Stage 2," and "Stage 3″ in Fig. 8(b), (d), and 8(e). It is worth mentioning that Huang et al. [59] divided the fretting fatigue diagram into the three mentioned parts and introduced the second region as a safer region for designers since the stress value in this region was far from the yield stress of the material compared to the first

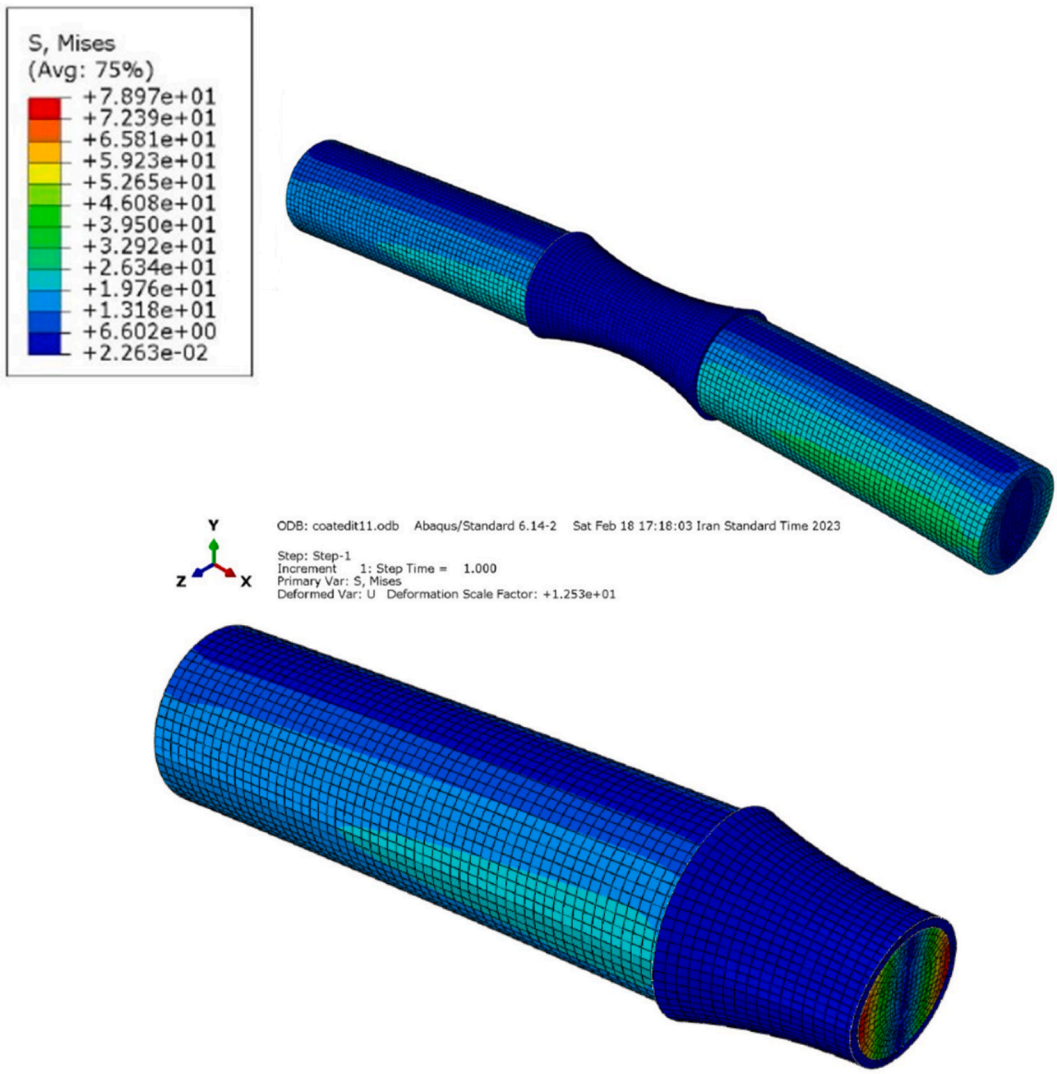

Fig. 7. Stress simulation in Abaqus software for coated sample.

Table 2
Mechanical properties used in the Abaqus software based on references [53,54].

Material	Elastic modulus (GPa)	Poisson ratio (−)
AM60	43.0 ± 2.6	0.35
PLA	3.7 ± 0.1	0.36

region. Even though cracks were initially detected at the highest wear rate in the slip regime (SR), the micro-cracks did not propagate during the nucleation phase and were eliminated, resulting in a slight increase in the fretting fatigue lifetime, which was an unexpected trend according to previous research by Parast and Azadi [56] and Peng et al. [57,58]. In order to identify the material properties, curve fitting was utilized in Fig. 8. The relationship between stress amplitude and fatigue lifetime can be expressed as follows [40,49]:

$$\sigma_a = \sigma_f^{'}\left(2N_f\right)^b \tag{1}$$

N_f represents the fatigue lifetime, while σ_a represents the stress amplitude, and $\sigma_f^{'}$ represents the fatigue strength coefficient. The fatigue strength exponent is denoted by b. To determine R^2 (the coefficient of determination) for all experimental data for both fretting fatigue and pure fatigue conditions (with and without PLA coating), regression analysis was conducted as shown in Fig. 8, and Table 3 displays the findings.

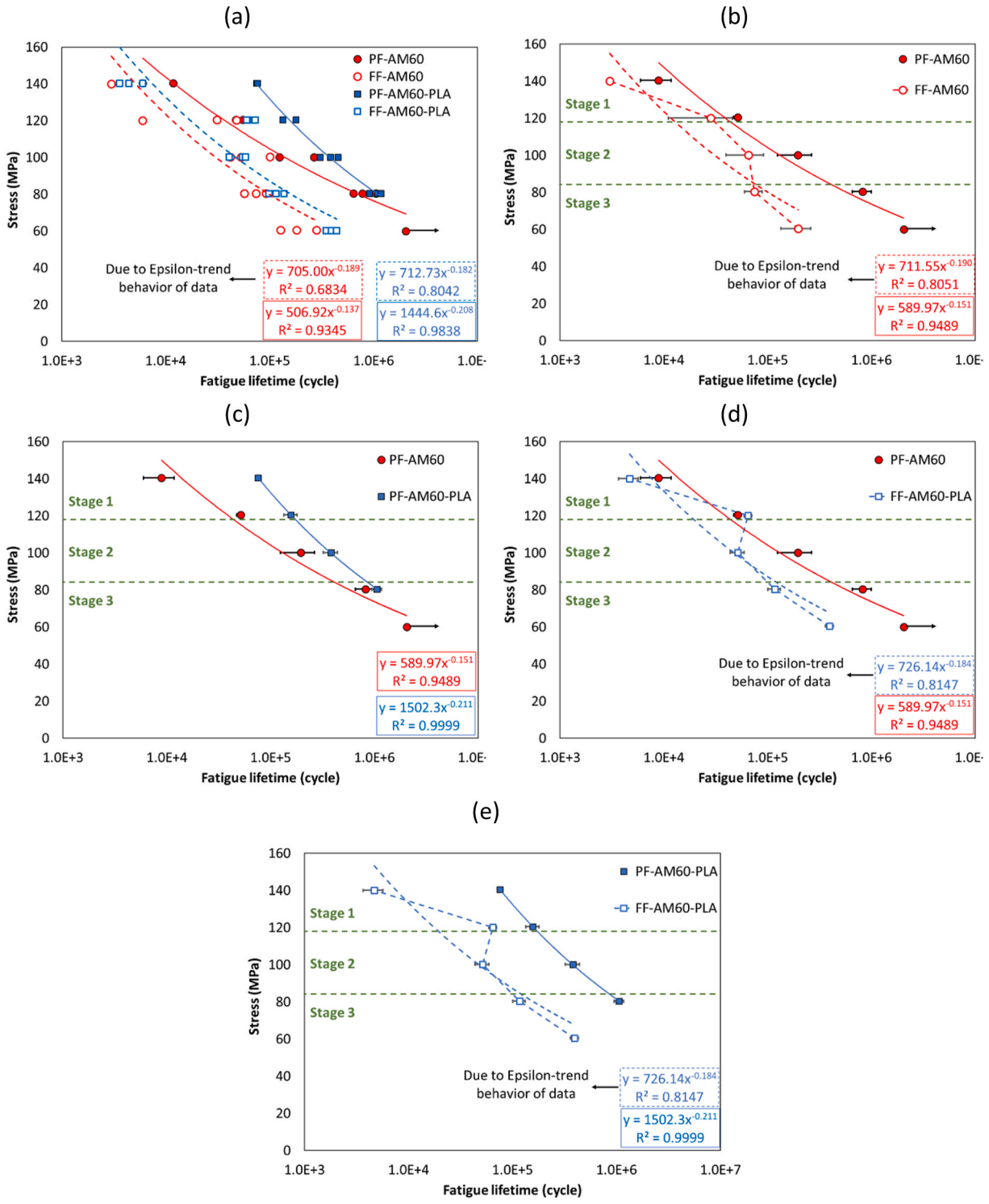

Fig. 8. The stress-lifetime (S–N) curves of AM60 magnesium alloy (coated and uncoated with PLA) under pure fatigue (PF) and fretting fatigue (FF) conditions ((a): for all data, (b): for average data (PF-AM60 and FF-AM60), (c): for average data (PF-AM60 and PF-AM60-PLA), (d): for average data (PF-AM60 and FF-AM60-PLA), and (e): for average data (PF-AM60-PLA and FF-AM60-PLA).

According to some researchers, an R^2 value greater than 90 % is considered acceptable for pure fatigue conditions [60]. The R^2 value for the fretting fatigue data is below 90 % due to the epsilon trend exhibited by the fretting fatigue condition. Table 4 presents the high-cycle fatigue properties of the AM60 magnesium alloy under both fretting and pure fatigue conditions. According to the

Table 3
The R^2 values for all data and average data in varying conditions.

Condition	Pure fatigue without coating (%)	Fretting fatigue without coating (%)	Pure fatigue with PLA coating (%)	Fretting fatigue with PLA coating (%)
R^2 (all data)	93	68	98	80
R^2 (average data)	94	80	99	81

information presented in Table 4, the coated samples subjected to pure fatigue testing demonstrated higher values of the fatigue strength coefficient ($\sigma_f^{'}$) and the fatigue strength exponent (b) compared to samples tested under other conditions. In pure fatigue conditions, the use of PLA coating resulted in a 154.64 % increase in the fatigue strength coefficient ($\sigma_f^{'}$) and a 39.73 % increase in the fatigue strength exponent (b) compared to uncoated samples, based on average data. Furthermore, in fretting fatigue conditions, the use of PLA coating led to a 2.05 % increase in the fatigue strength coefficient ($\sigma_f^{'}$) and a 3.15 % decrease in the fatigue strength exponent (b) compared to uncoated samples, based on average data.

3.2. Fracture analysis

FESEM was used to analyze the fracture surface of AM60 and characterize its failure characteristics. Specimens with and without PLA coating were chosen for testing under fretting and pure fatigue conditions at 80 MPa and 120 MPa stress to determine failure values. The results for 80 MPa are shown in Fig. 9(a): Pure fatigue without PLA coating, Fig. 9(b): Pure fatigue with PLA coating, Fig. 9 (c): Fretting fatigue without PLA coating, and Fig. 9(d): Fretting fatigue with PLA coating, while the results for 120 MPa are shown in Fig. 9(e): Pure fatigue without PLA coating, Fig. 9(f): Pure fatigue with PLA coating, Fig. 9(g): Fretting fatigue without PLA coating, and Fig. 9(h): Fretting fatigue with PLA coating.

The fatigue failure in hexagonally close-packed (HCP) metals, such as titanium alloys [61] and magnesium alloys [62,63], often results in the observation of faceted morphologies in fractography. The occurrence of faceted morphologies can be attributed to quasi-cleavage fracture that takes place along the appropriate crystal planes. Another crucial observation in Fig. 9(c), (d), 9(g), and 9 (h) is the presence of the fretting area. This area was more extensive in the specimen with an 80 MPa stress level. In contrast, it was relatively small in the specimen with a 120 MPa stress level, indicating that the fatigue phenomenon was the primary cause of failure, rather than fretting fatigue. This point was also mentioned in the previous research [49]. Fig. 9(a), (b), 9(e), and 9(f) show fracture surfaces with high magnification, which include both samples with and without PLA coating. In Fig. 9(b) and (f), which are related to the samples with PLA coating and at the stress level of 80 and 120 MPa, respectively; PLA layers and parts of it that have separated from the AM60 magnesium alloy have been made, it can be seen and also the casting defect and the created cracks are also clear in these pictures. In the samples without PLA coating and under pure fatigue, as shown in Fig. 9(a) and (e), cracks starting from the surface of the sample (near the edge) or approximately in the middle of the sample can be seen, as well. Besides, casting defects were also observed. Fatigue cracks can generally initiate at stress concentration sites such as the defects created during manufacturing (e.g., shrinkage voids, pores, and inclusions formed during casting, or surface defects, such as notches, and corners that develop during machining) [64,65]. More details are mentioned in Figs. 10–13 and with images with higher magnifications.

The images in Figs. 10–13 depict a fracture surface with flat cleavage planes featuring striation-like patterns. The rough areas indicate where the crack has grown, and the surfaces appear randomly oriented and serrated. Similar characteristics were observed in high-cycle fatigue analysis of a fracture surface in a cast AM60 alloy [26]. One research [26] found that on flat cleavage planes with striation-like patterns, transgranular crack growth occurred through dendrite cells, whereas intergranular crack growth occurred through interdendritic arms containing β-$Mg_{17}Al_{12}$ particles, which resulted in rough regions with randomly oriented serrated surfaces. When the stress intensity component, which is responsible for crack growth, increased and caused the transition from the former crack development mechanism to the latter, there was a change in the brightness of the fracture surfaces. The question of whether the β particles were debonded or caused premature fracture was used as an explanation for whether the driving force was sufficient [13,40]. According to a study by Hashemi et al. [66], the majority of facets on the specimen fracture surface were found to be intergranular. The presence of intergranular facets significantly reduces the rate of crack propagation. This phenomenon can be attributed to the increased tortuosity caused by the crack path and the deviation of the crack from the maximum stress plane.

In the absence of any flaws in the cast microstructure, the stress concentrators for initiating fatigue cracks are the slip markings

Table 4
The fatigue properties of AM60 alloys.

Condition	Using all experimental data		Using averaged values	
	$\sigma_f^{'}$ (MPa)	b (−)	$\sigma_f^{'}$ (MPa)	b (−)
Pure fatigue without PLA coating	506.92	−0.137	589.97	−0.151
Fretting fatigue without PLA coating	705.00	−0.189	711.55	−0.190
Pure fatigue with PLA coating	1444.60	−0.208	1502.30	−0.211
Fretting fatigue with PLA coating	712.73	−0.182	726.14	−0.184

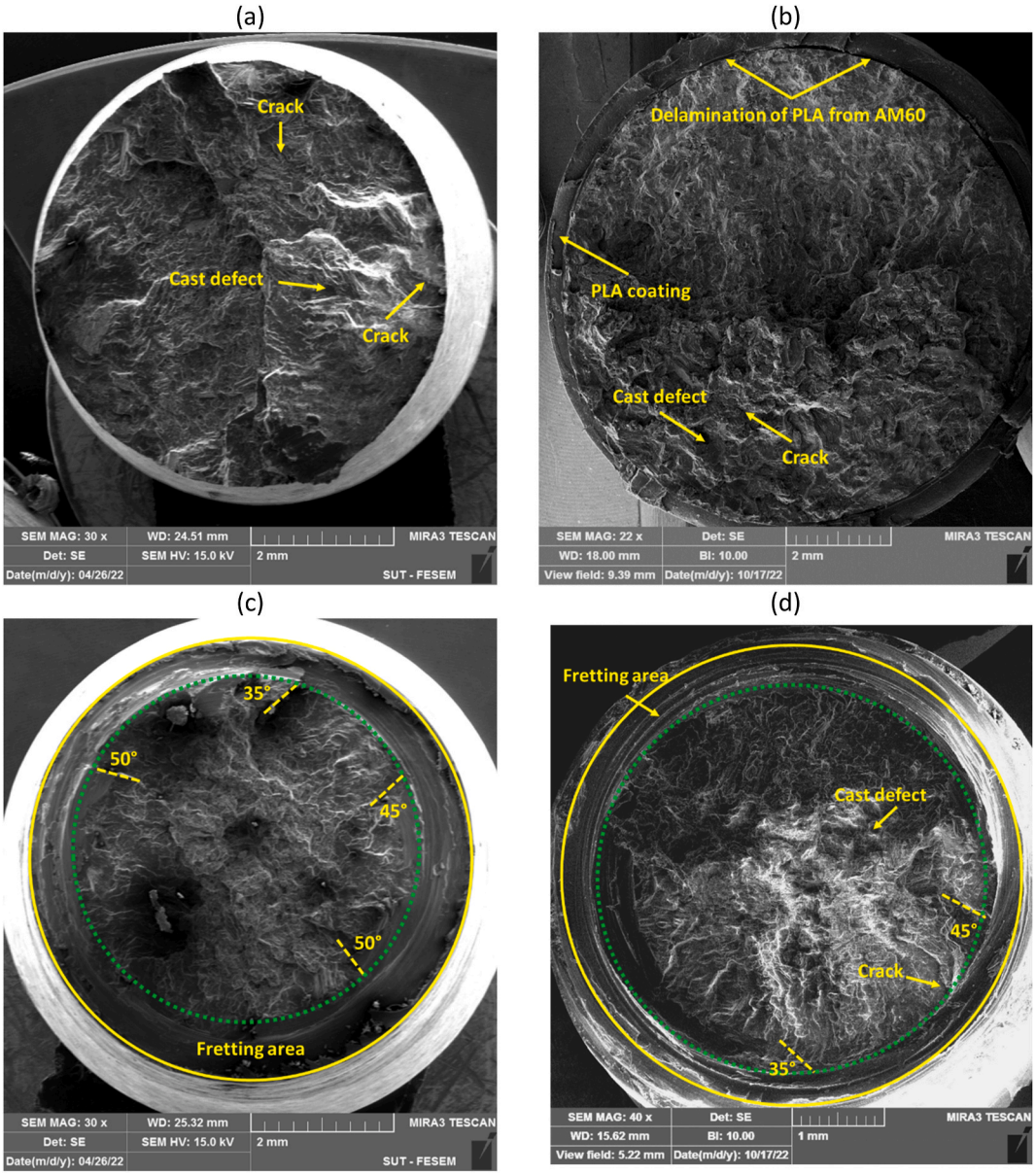

Fig. 9. The fracture surface at the stress level of 80 MPa under (a) pure fatigue without PLA coating, (b) pure fatigue with PLA coating, (c) fretting fatigue without PLA coating, and (d) fretting fatigue with PLA coating condition and the fracture surface at the stress level of 120 MPa under (e) pure fatigue without PLA coating, (f) pure fatigue with PLA coating, (g) fretting fatigue without PLA coating, and (h) fretting fatigue with PLA coating condition

(SMs) that indicate the localization of cyclic plastic deformation in the solid solution regions. This is highlighted in Refs. [34,67]. According to the research by Dimitrov et al. [68], the initiation of possible fatigue cracks is at the interface between the $Mg_{17}Al_{12}$ phase particles and the solid solution matrix. In the high-cycle fatigue regime (stress level 120 MPa), the initiation of fatigue cracks on the fractured particles of $Mg_{17}Al_{12}$ was the main mechanism responsible for the specimen failure. The intensity of the formation and evolution of SMs leading to crack initiation is mainly dependent on the applied stress amplitude [69]. The relief that was created led to the concentration of intense stress in the SMs, which in turn resulted in the initiation of fatigue cracks. Since most of the energy for plastic deformation was released through the formation of the SMs, the cracks initiated at the interfaces between brittle intermetallic particles and the solid solution. In certain instances, the cracks were observed to propagate from the fractured particles into the solid solution [69]. However in the low-cycle fatigue regime (at a stress level of 80 MPa), only a few instances of SMs formation were observed. However, the initiation of cracks on SMs was accompanied by the propagation of cracks formed in the intermetallic particles [70–72]. This phenomenon was not typically observed at higher testing stress amplitudes. Figs. 11 and 13 provide evidence of wear

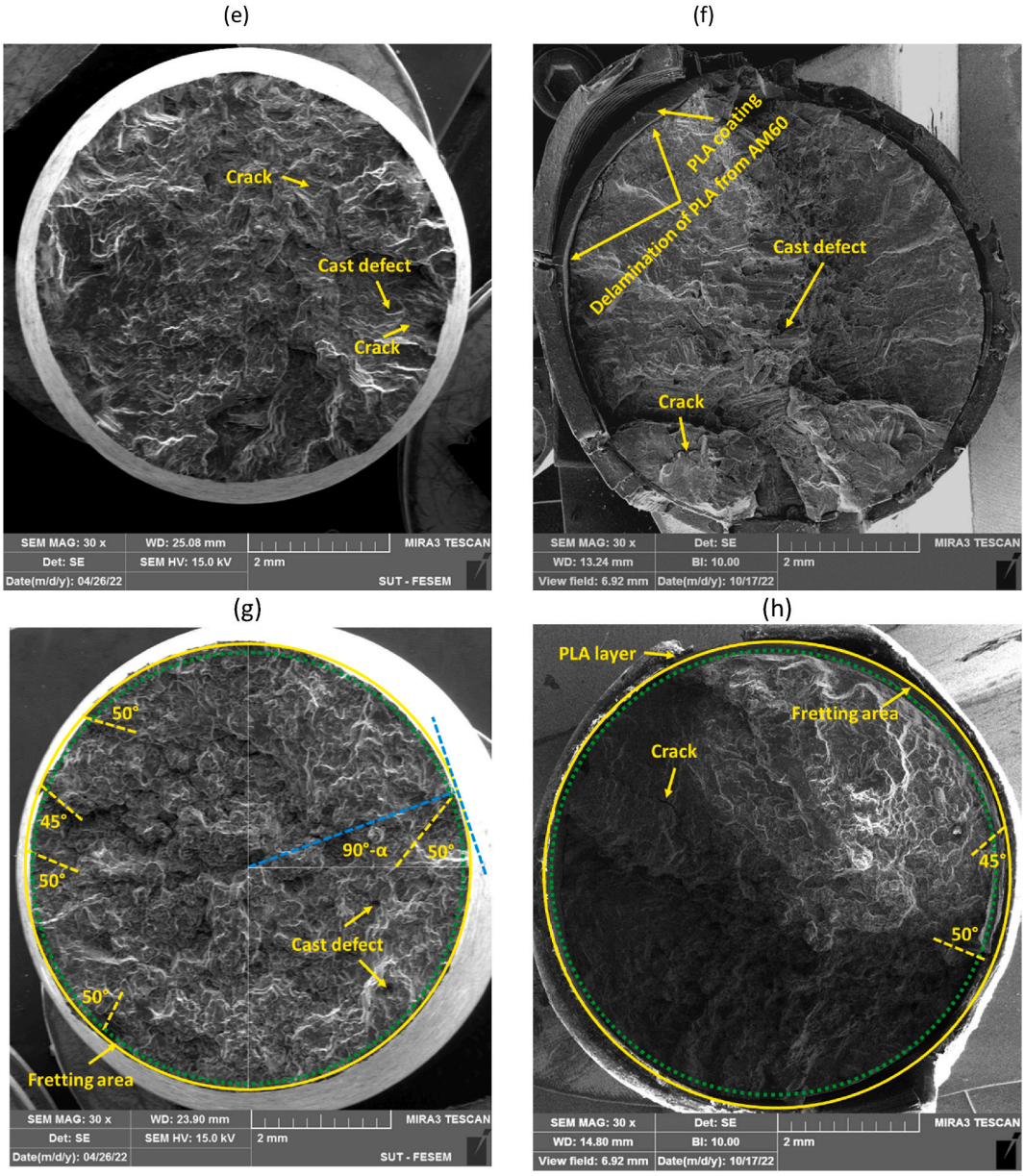

Fig. 9. (*continued*).

and the impact of fretting near the contact edge with the pads. This particular type of failure surface related to fretting fatigue conditions was also reported by Sadeler and Atasoy [31]. The initiation angle of the fretting fatigue crack propagation in Fig. 9(c), (d), 9 (g), and 9(h) was observed to be between 35 and 50°. This angle is consistent with the results obtained by Peng et al. [57,73], who found that the fretting fatigue crack initiation angle is about 30° towards the surface. In this study, as the loading conditions were bending, the surface of the sample experienced the highest stress. Therefore, most of the fatigue cracks are initiated near the surface. This finding is consistent with the findings of Nascimento et al. [74], Oliya et al. [42], and Song et al. [75]. Moreover, the region near the contact surface is also susceptible to fretting fatigue cracks formation, as contact stresses experience their highest local values in this area, owing to stress concentration. As per the literature [56], wear fatigue loading conditions result in stress concentration leading to faster crack propagation and quicker formation of fractures, which ultimately causes a shorter fretting fatigue lifetime. Wear fatigue crack growth is primarily caused by the wedge effect, where the entry of wear debris into small cracks accelerates the propagation of cracks, as stated in Ref. [56]. If the debris oxidizes due to friction heating and becomes potentially abrasive, it will increase the likelihood of the crack initiation [76]. The total wear in the fretting fatigue condition is the sum of delamination, abrasion, oxidation, and adhesion [77].

Fig. 9(c) and (d) show visible wear damage on the edge of the sample. Figs. 10–13 exhibit the presence of porosity resulting from

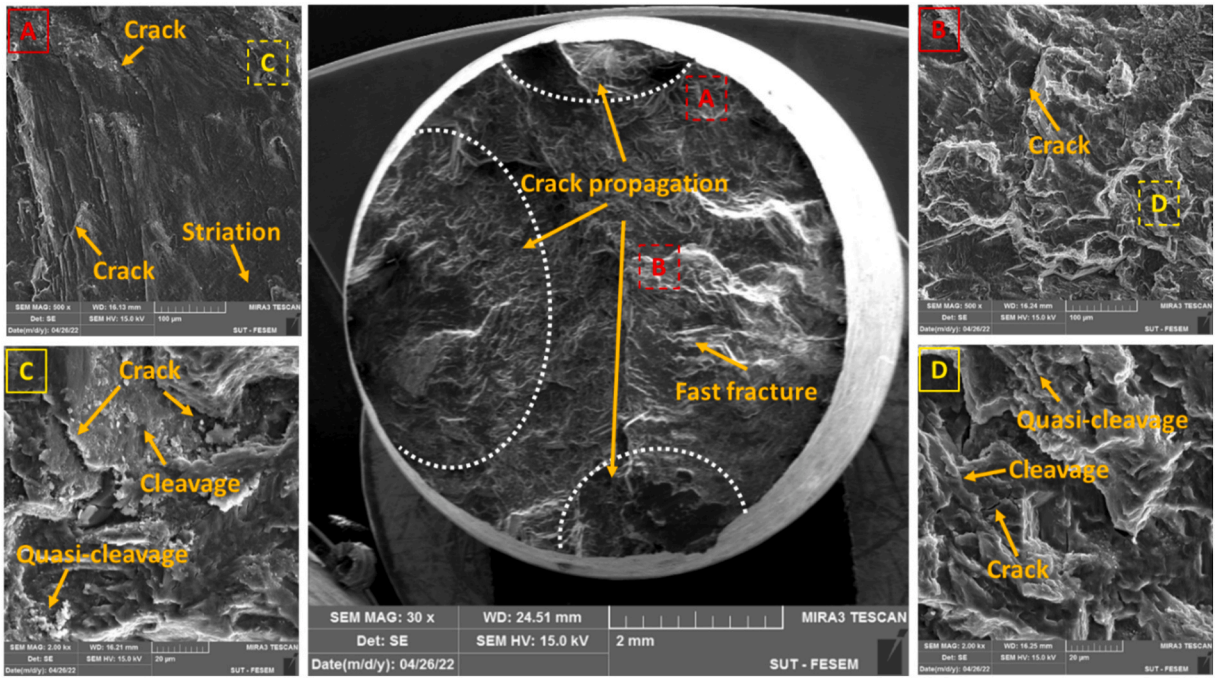

Fig. 10. The surface fracture under PF conditions with a stress level of 80 MPa.

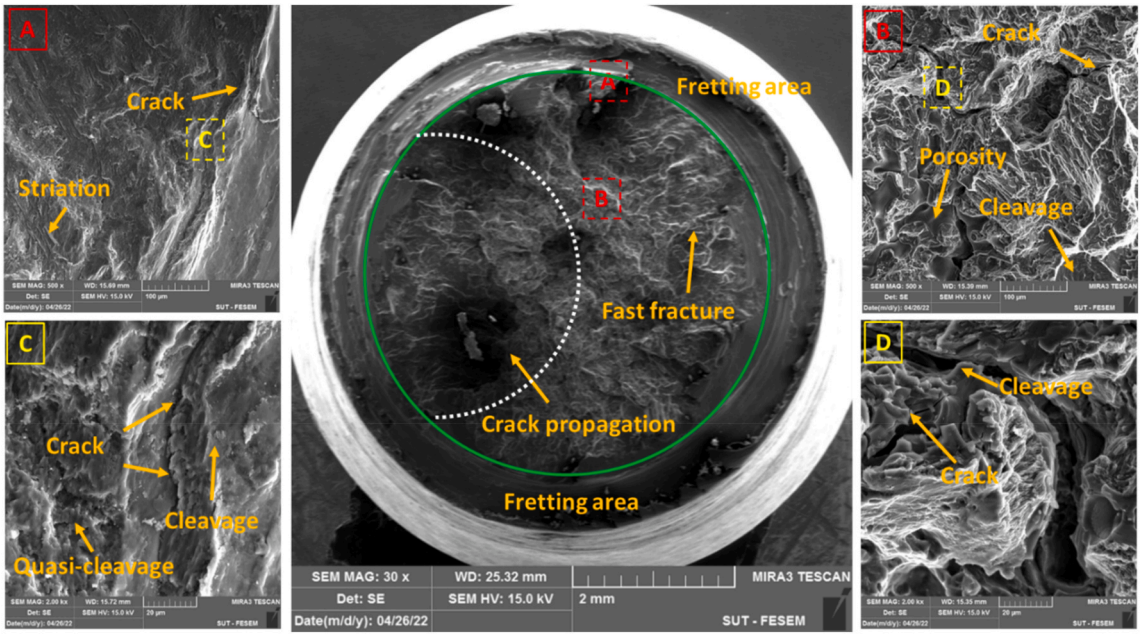

Fig. 11. The surface fracture under FF conditions with a stress level of 80 MPa.

casting defects in some cases. These defects can cause a decrease in fatigue lifetime and serve as a region for the onset of cracks. Previous studies have also identified casting defects as the main cause of fatigue crack initiation and specimen failure in most cases [34, 78–80]. By comparing the fatigue fracture surface of the fretting fatigue and pure fatigue, it was observed that the effects of cleavage increased in the fatigue fracture surface of the fretting fatigue, which indicates the brittleness of the fracture [81]. By observing the shapes of the fracture surface related to fretting fatigue, it was found that wear damage is applied to the surface of the sample and some areas near the edge of the surface are severely damaged and deformed [82,83]. In relation to the fracture surface of fretting fatigue samples according to Peng et al. [73], the contact normal stress level mostly controls the crack formation and initial crack growth

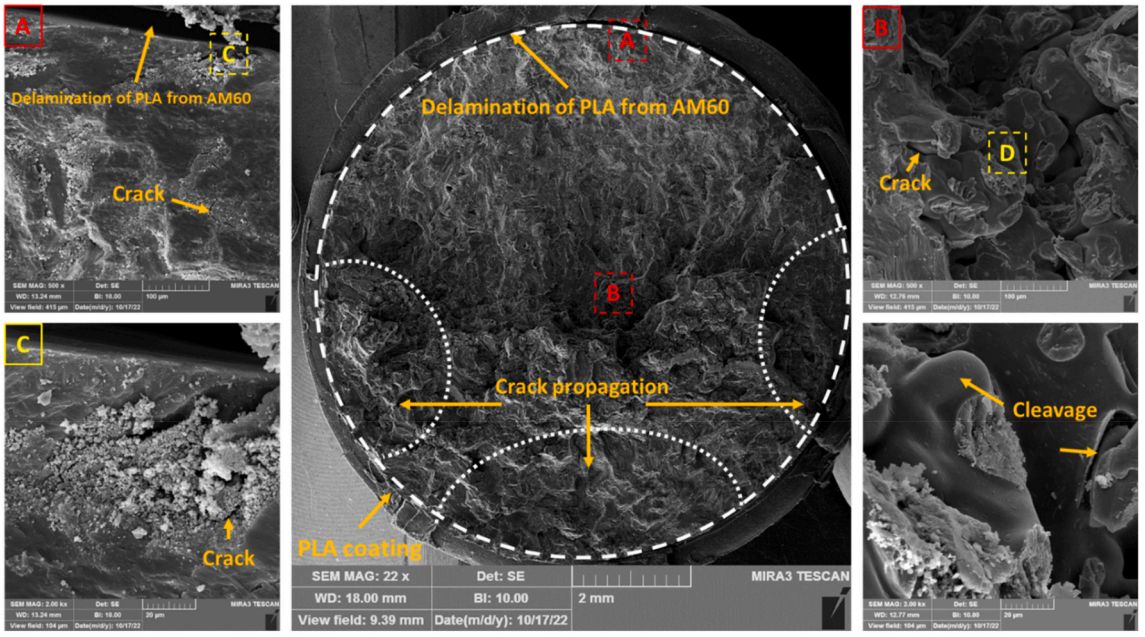

Fig. 12. The surface fracture under PF conditions with a stress level of 80 MPa (with PLA coating).

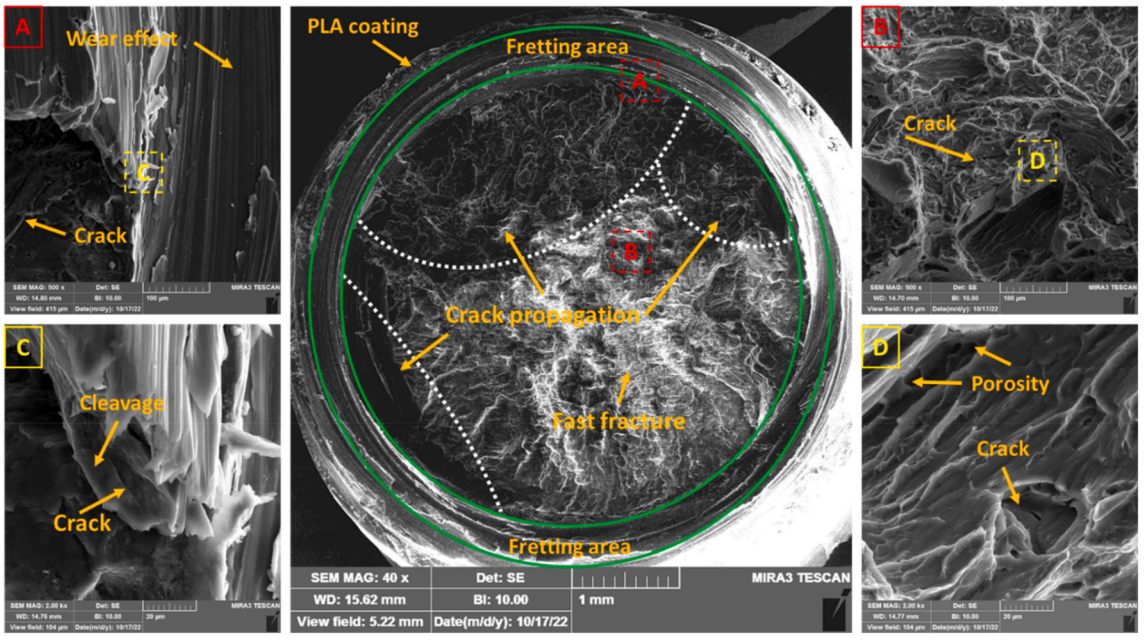

Fig. 13. The surface fracture under FF conditions with a stress level of 80 MPa (with PLA coating).

angle, but the crack growth is controlled by the stress level. Fig. 13 shows the surface of the worn in a clear manner. Besides, Fig. 13 illustrates the mechanism of delamination wear. The separation of material as a result of fractures that occur perpendicular to the direction of sliding is the hallmark of the delamination wear mechanism. Since the majority of magnesium alloys have limited cold ductility, even at modest loads, the worn surface significantly hardens. The continual deformation of the material embrittles its surface and is the cause of perpendicular fissures to the sliding direction, which release sheet-like pieces of the worn material, even with alloys with higher ductility, such as the AM60B studied in another work [84].

In coated samples, under the fretting fatigue condition test, the PLA layer was destroyed due to wear and could not be imaged to present the fracture surface, but in the coated sample under pure fatigue test (Fig. 12), the PLA layer connected to AM60 magnesium

alloy in Some areas are clear, also delamination between PLA and AM60 magnesium alloy is evident in these figures. All of the samples exhibit brittle fracture behavior, with the presence of both cleavage and quasi-cleavage being observed.

Table 5 displays the quantity and size of microcracks of coated and uncoated samples with PLA, in fretting fatigue and pure fatigue circumstances. Findings in Table 5 reveal that the mean length of cracks is greater at higher stress levels in both testing conditions (pure fatigue and fretting fatigue) and coated and uncoated samples, than at lower stress levels. It is worth noting that the fatigue lifetime (with and without coating) at the high-stress level is lower than the fatigue lifetime at the low-stress level. PLA coating caused the number of cracks to decrease by 35.55 and 61.53 %, respectively, in pure fatigue test conditions at both low and high-stress levels, which is one of the reasons for increasing the lifetime of coated samples. In the condition of fretting fatigue, in both low and high-stress levels, PLA coating reduced the number of cracks by 51.65 % and 40 %, respectively.

The fracture surfaces of the material were investigated utilizing EDX map analysis. Fig. 14 shows the EDX analysis of a fretting fatigue test sample with PLA coating at a stress level of 80 MPa. Fig. 14 clearly depicts the presence of both magnesium and intermetallic phases on the fracture surfaces of all samples. In Fig. 14, the hues orange, purple, and blue represent the elements Mg, Al, and Mn, respectively.

Based on the findings of Horstemyer et al. [26] and as shown in Fig. 14, intermetallic phases have been identified as potential sites for microcrack initiation. Specifically, microcracks tend to form near intermetallic deposits, with the Mg–Al intermetallics being the most significant, followed by Al–Mn intermetallics, eventually leading to the final failure. Microcracks were observed to initiate from the $Mg_{17}Al_{12}$ intermetallic phase in the magnesium matrix, as shown in Fig. 14. According to Mokhtarishirazabad et al. [85], the presence of the $Mg_{17}Al_{12}$ phase can lead to a reduction in strength, especially at elevated temperatures.

4. Conclusions

This article provides the fretting fatigue and pure fatigue properties of AM60 magnesium alloy (cast), including its performance both with and without a PLA coating that was 3D-printed and a summary of results could be mentioned as follows,

- The fretting fatigue lifetime of uncoated samples was observed to decrease by 44.8 % and 91 % at the maximum stress level (120 MPa) and the lowest stress level (80 MPa), respectively, compared to the pure fatigue condition.
- Fretting fatigue caused a reduction in the lifetime of coated samples under the lowest stress (80 MPa) and maximum stress (120 MPa) by 56 % and 88 %, respectively, when compared to conditions of pure fatigue.
- When subjected to fretting fatigue conditions, the material properties of uncoated samples exhibited an increase in both the fatigue strength coefficient and exponent, as observed in both the averaged and all experimental data. The fatigue strength coefficient ($\sigma_f^{'}$) was found to improve fretting fatigue loading by approximately 39 % when compared to pure fatigue. Furthermore, the absolute value of the fatigue strength exponent (b) was observed to increase by 37.9 % in comparison to pure fatigue.
- In the pure fatigue test, the PLA coating resulted in a significant increase in material properties such as fatigue strength coefficient and exponent. The increase was 184.97 % and 51.82 % (using all data results) and 154.64 % and 39.73 % (using the average data results), respectively.
- The S–N diagram for fretting fatigue exhibits an epsilon-shaped curve. It has been observed that the lifetime of fretting fatigue decreases as the stress level is increased, except when the stress level is below 120 MPa.
- Under the fretting fatigue test, PLA coating increased the fatigue strength exponent by 1.09 % (using the results of all data) and 2.05 % (using the average results of the data). While the fatigue strength coefficient decreased by 3.70 % (using the results of all data) and 3.15 % (using the average data results).
- The AM60 magnesium alloy exhibited brittle fracture characteristics, possibly attributed to the existence of cleavage and quasi-cleavage traits on the fracture surface of the specimens.
- The lifetime of AM60 can be extended by using PLA coating. This coating has been found to reduce cracks by 35.55 % and 61.53 % in pure fatigue tests under low and high stress levels respectively. Additionally, fretting fatigue tests have shown a decrease in cracks of 51.65 % and 40 % under low and high stress levels respectively as a result of the application of PLA coating.

Data availability statement

The raw data that support the findings of this research are available based on a reasonable request from the corresponding author. In general, these experimental data are not publicly available due to some restrictions.

Table 5
The length and the number of micro-cracks based on 2000X FESEM images (in the crack propagation region).

Stress level	Pure fatigue without coating		Fretting fatigue without coating		Pure fatigue with PLA coating		Fretting fatigue with PLA coating	
	Number	Length (μm)	Number	Length (μm)	Number	Length (μm)	Number	Length (μm)
80 MPa	45	4.96 ± 2.95	15	17.83 ± 22.36	29	7.97 ± 0.40	10	10.25 ± 4.37
120 MPa	39	7.41 ± 4.20	11	23.18 ± 17.72	15	13.70 ± 8.82	9	15.61 ± 4.76

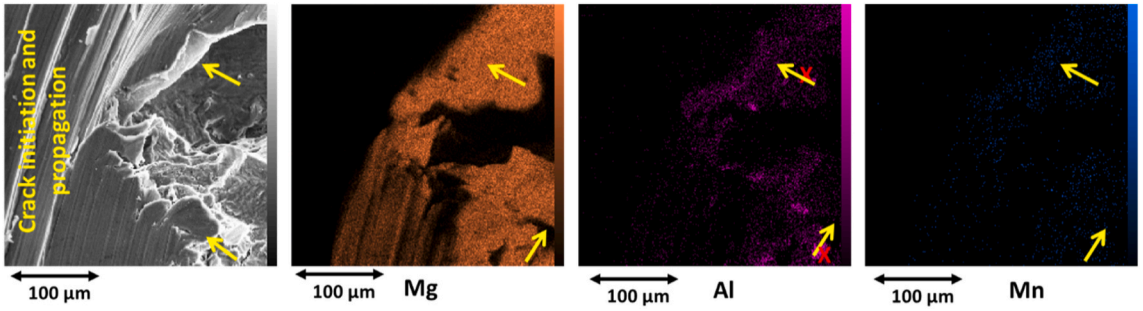

Fig. 14. FE-SEM images with the EDX analysis of fracture surfaces (Note: The arrows start, and indicate the beginning of the crack and the direction in which it spreads. Additionally, the letter "X" represents the level of intermetallic phases present in the area where the crack first appears.).

CRediT authorship contribution statement

Saeid Rezanezhad: Writing – original draft, Visualization, Software, Resources, Methodology, Investigation, Formal analysis, Data curation. **Mohammad Azadi:** Writing – review & editing, Visualization, Validation, Supervision, Resources, Project administration, Methodology, Investigation, Funding acquisition, Conceptualization.

Declaration of competing interest

The authors declare that they have no known competing financial interests or personal relationships that could have appeared to influence the work reported in this paper.

References

[1] D. Mangardich, F. Abrari, Z. Fawaz, A fracture mechanics based approach for the fretting fatigue of aircraft engine fan dovetail attachments, Int. J. Fatig. 129 (2019) 105213.
[2] A. Parast, M.H. Haji Esmaeili, M. Azadi, Comparing bending fatigue and fretting fatigue properties in aluminum-silicon alloy under working conditions of engine piston-ring system, J. Solid Fluid Mech. 11 (2021) 157–174.
[3] I. Milne, R.O. Ritchie, B.L. Karihaloo, Comprehensive Structural Integrity: Cyclic Loading and Fatigue, vol. 4, Elsevier, 2003.
[4] S.L. Sunde, F. Berto, B. Haugen, Predicting fretting fatigue in engineering design, Int. J. Fatig. 117 (2018) 314–326.
[5] D.A. Hills, D. Nowell, Mechanics of fretting fatigue—oxford's contribution, Tribol. Int. 76 (2014) 1–5.
[6] H.M. Mousa, A. Abdal-hay, M. Bartnikowski, I.M.A. Mohamed, A.S. Yasin, S. Ivanovski, et al., A multifunctional zinc oxide/poly(lactic acid) nanocomposite layer coated on magnesium alloys for controlled degradation and antibacterial function, ACS Biomater. Sci. Eng. 4 (2018) 2169–2180, https://doi.org/10.1021/acsbiomaterials.8b00277.
[7] J. Wang, X. Pang, H. Jahed, Surface protection of Mg alloys in automotive applications: a review, AIMS Mater Sci 6 (2019) 567–600, https://doi.org/10.3934/matersci.2019.4.567.
[8] N. Scharnagl, C. Blawert, W. Dietzel, Corrosion protection of magnesium alloy AZ31 by coating with poly(ether imides) (PEI), Surf. Coating. Technol. 203 (2009) 1423–1428, https://doi.org/10.1016/j.surfcoat.2008.11.018.
[9] L. Yang, E. Zhang, Biocorrosion behavior of magnesium alloy in different simulated fluids for biomedical application, Mater. Sci. Eng. C 29 (2009) 1691–1696.
[10] X.N. Gu, X.L. Li, W.R. Zhou, Y. Cheng, Y.F. Zheng, Microstructure, biocorrosion, and cytotoxicity evaluations of rapid solidified Mg–3Ca alloy ribbons as a biodegradable material, Biomed. Mater. 5 (2010) 35013.
[11] M.P. Staiger, A.M. Pietak, J. Huadmai, G. Dias, Magnesium and its alloys as orthopedic biomaterials: a review, Biomaterials 27 (2006) 1728–1734.
[12] Y. Shi, M. Qi, Y. Chen, P. Shi, MAO-DCPD composite coating on Mg alloy for degradable implant applications, Mater. Lett. 65 (2011) 2201–2204.
[13] J. Sun, G. Wang, Preparation and corrosion resistance of cerium conversion coatings on AZ91D magnesium alloy by a cathodic electrochemical treatment, Surf. Coating. Technol. 254 (2014) 42–48.
[14] M.P. Sealy, Y.B. Guo, Surface integrity and process mechanics of laser shock peening of novel biodegradable magnesium–calcium (Mg–Ca) alloy, J. Mech. Behav. Biomed. Mater. 3 (2010) 488–496.
[15] X.N. Gu, W. Zheng, Y. Cheng, Y.F. Zheng, A study on alkaline heat treated Mg–Ca alloy for the control of the biocorrosion rate, Acta Biomater. 5 (2009) 2790–2799.
[16] M. Razavi, M. Fathi, O. Savabi, D. Vashaee, L. Tayebi, Micro-arc oxidation and electrophoretic deposition of nano-grain merwinite (Ca3MgSi2O8) surface coating on magnesium alloy as biodegradable metallic implant, Surf. Interface Anal. 46 (2014) 387–392.
[17] R.O. Hussein, D.O. Northwood, X. Nie, The effect of processing parameters and substrate composition on the corrosion resistance of plasma electrolytic oxidation (PEO) coated magnesium alloys, Surf. Coating. Technol. 237 (2013) 357–368.
[18] R. Rojaee, M. Fathi, K. Raeissi, Controlling the degradation rate of AZ91 magnesium alloy via sol–gel derived nanostructured hydroxyapatite coating, Mater. Sci. Eng. C 33 (2013) 3817–3825.
[19] Y. Ren, E. Babaie, S.B. Bhaduri, Nanostructured amorphous magnesium phosphate/poly (lactic acid) composite coating for enhanced corrosion resistance and bioactivity of biodegradable AZ31 magnesium alloy, Prog. Org. Coating 118 (2018) 1–8, https://doi.org/10.1016/j.porgcoat.2018.01.014.
[20] P. Shi, B. Niu, S. E, Y. Chen, Q. Li, Preparation and characterization of PLA coating and PLA/MAO composite coatings on AZ31 magnesium alloy for improvement of corrosion resistance, Surf. Coating. Technol. 262 (2015) 26–32, https://doi.org/10.1016/j.surfcoat.2014.11.069.
[21] L. Xu, A. Yamamoto, Characteristics and cytocompatibility of biodegradable polymer film on magnesium by spin coating, Colloids Surf. B Biointerfaces 93 (2012) 67–74.
[22] H. Hornberger, S. Virtanen, A.R. Boccaccini, Biomedical coatings on magnesium alloys–a review, Acta Biomater. 8 (2012) 2442–2455.
[23] M. Azadi, S. Rezanezhad, S.A. Ashraf Talesh, K. Ivanov, A. Teresov, The effect of pulsed electron beam irradiation on surface characteristics of AM60 magnesium alloy, Prog Phys Appl Mater 1 (2021) 63–73.
[24] M. Azadi, K. Ivanov, S. Rezanezhad, S.A.A. Talesh, Scanning and transmission electron microscopy analysis for surface-modified AM60 magnesium alloy by pulsed electron beam irradiation, Nucl. Instrum. Methods Phys. Res. Sect. B Beam Interact. Mater. Atoms 513 (2022) 9–13.

[25] Z. Chen, A. Shyam, J. Huang, R.F. Decker, S.E. LeBeau, C.J. Boehlert, The small fatigue crack growth behavior of an AM60 magnesium alloy, Metall. Mater. Trans. A 44 (2013) 1045–1058, https://doi.org/10.1007/s11661-012-1449-1.
[26] M.F. Horstemeyer, N. Yang, K. Gall, D. McDowell, J. Fan, P. Gullett, High cycle fatigue mechanisms in a cast AM60B magnesium alloy, Fatig. Fract. Eng. Mater. Struct. 25 (2002) 1045–1056.
[27] K. Gall, G. Biallas, H.J. Maier, P. Gullett, M.F. Horstemeyer, D.L. McDowell, et al., In-situ observations of high cycle fatigue mechanisms in cast AM60B magnesium in vacuum and water vapor environments, Int. J. Fatig. 26 (2004) 59–70.
[28] K. Tokaji, M. Kamakura, Y. Ishiizumi, N. Hasegawa, Fatigue behaviour and fracture mechanism of a rolled AZ31 magnesium alloy, Int. J. Fatig. 26 (2004) 1217–1224.
[29] K. Gall, G. Biallas, H.J. Maier, M.F. Horstemeyer, D.L. McDowell, Environmentally influenced microstructurally small fatigue crack growth in cast magnesium, Mater. Sci. Eng., A 396 (2005) 143–154.
[30] M. Papakyriacou, H. Mayer, U. Fuchs, S.E. Stanzl-Tschegg, R.P. Wei, Influence of atmospheric moisture on slow fatigue crack growth at ultrasonic frequency in aluminium and magnesium alloys, Fatig. Fract. Eng. Mater. Struct. 25 (2002) 795–804.
[31] R. Sadeler, S. Atasoy, The effect of contact pad hardness on the fretting fatigue behaviour of AZ61 magnesium alloy, Fatig. Fract. Eng. Mater. Struct. 39 (2016) 502–510, https://doi.org/10.1111/ffe.12387.
[32] T.O. Olugbade, B.O. Omiyale, O.T. Ojo, Corrosion, corrosion fatigue, and protection of magnesium alloys: mechanisms, measurements, and mitigation, J. Mater. Eng. Perform. 31 (2022) 1707–1727, https://doi.org/10.1007/s11665-021-06355-2.
[33] L.D. Pîrvulescu, A.V. Cernescu, C. Opriș, L. Marșavina, Size effect in fatigue life of Mg alloy, Procedia Struct. Integr. 41 (2022) 492–499.
[34] G. Eisenmeier, B. Holzwarth, H.W. Höppel, H. Mughrabi, Cyclic deformation and fatigue behaviour of the magnesium alloy AZ91, Mater. Sci. Eng., A 319 (2001) 578–582.
[35] Q. Li, Q. Yu, J. Zhang, Y. Jiang, Effect of strain amplitude on tension–compression fatigue behavior of extruded Mg6Al1ZnA magnesium alloy, Scripta Mater. 62 (2010) 778–781.
[36] L.H. Rettberg, J.B. Jordon, M.F. Horstemeyer, J.W. Jones, Low-cycle fatigue behavior of die-cast Mg alloys AZ91 and AM60, Metall. Mater. Trans. A 43 (2012) 2260–2274.
[37] S. Rezanezhad, M. Azadi, Impact of 3D-printed PLA coatings on the mechanical and adhesion properties of AM60 magnesium alloys, Compos Part C Open Access 12 (2023) 100415, https://doi.org/10.1016/j.jcomc.2023.100415.
[38] M. Azadi, A. Dadashi, S. Dezianian, M. Kianifar, S. Torkaman, M. Chiyani, High-cycle bending fatigue properties of additive-manufactured ABS and PLA polymers fabricated by fused deposition modeling 3D-printing, Forces Mech 3 (2021) 100016, https://doi.org/10.1016/j.finmec.2021.100016.
[39] N. Naveed, Investigating the material properties and microstructural changes of fused filament fabricated PLA and tough-PLA parts, Polymers 13 (2021) 1487.
[40] M. Azadi, S. Rezanezhad, M. Zolfaghari, Effect of simultaneous use of silica nanoparticles and heat treatment on high-cycle bending fatigue lifetime in piston aluminum alloy, Modares Mech Eng 20 (2020) 1463–1473.
[41] M.S. Bhuiyan, Y. Mutoh, T. Murai, S. Iwakami, Corrosion fatigue behavior of extruded magnesium alloy AZ61 under three different corrosive environments, Int. J. Fatig. 30 (2008) 1756–1765.
[42] A.Y.P. Oliya, M. Azadi, M.S.A. Parast, M. Mokhtarishirazabad, Effect of heat-treating on microstructure and high cycle bending fatigue behavior of AZ91 and AZE911 magnesium alloys, Adv. Mater. Sci. Eng. 2022 (2022) 1–11, https://doi.org/10.1155/2022/4030062.
[43] A.A.D. Sarhan, E. Zalnezhad, M. Hamdi, The influence of higher surface hardness on fretting fatigue life of hard anodized aerospace AL7075-T6 alloy, Mater. Sci. Eng., A 560 (2013) 377–387.
[44] E. Zalnezhad, A.A.D. Sarhan, P. Jahanshahi, A new fretting fatigue testing machine design, utilizing rotating–bending principle approach, Int. J. Adv. Manuf. Technol. 70 (2014) 2211–2219.
[45] R.W. Neu, Progress in standardization of fretting fatigue terminology and testing, Tribol. Int. 44 (2011) 1371–1377.
[46] M. Azadi, M. Zolfaghari, M.H. Hajiesmaeili, S. Rezanezhad. Fretting Fatigue Test Machine With Functionality In Lubricant And High Temperature, 2019. Patent Number: 98399, Int Categ: G01N/34, Intellectual Property Organization of Iran.
[47] M. Takiguchi, H. Ando, T. Takimoto, A. Uratsuka, Characteristics of friction and lubrication of two-ring piston, JSAE Rev. 17 (1996) 11–16.
[48] M.K. Ahmed Ali, H. Xianjun, R. Fiifi Turkson, M. Ezzat, An analytical study of tribological parameters between piston ring and cylinder liner in internal combustion engines, Proc. Inst. Mech. Eng. - Part K J. Multi-body Dyn. 230 (2016) 329–349.
[49] S. Rezanezhad, M. Azadi, Amazing epsilon-shaped trend for fretting fatigue characteristics in AM60 magnesium alloy under stress-controlled cyclic conditions at bending loads with zero mean stress, PLoS One 18 (2023) e0281263.
[50] P. Linde, J. Pleitner, H. de Boer, C. Carmone, Modelling and Simulation of Fibre Metal Laminates. ABAQUS Users Conf, 2004.
[51] C. Bedon, K. Machalická, M. Eliášová, M. Vokáč, Numerical modelling of adhesive connections including cohesive damage, Challenging Glas 6 Conf Archit Struct Appl Glas CGC 2018 - Proc (2018) 309–320, https://doi.org/10.7480/cgc.6.2155.
[52] H. Alshahrani, A. Ahmed, Study on flexural behavior of glass fiber reinforced plastic sandwich composites using liquid thermoplastic resin, Polymers 14 (2022) 4045, https://doi.org/10.3390/polym14194045.
[53] F. Samadpour, G. Faraji, A. Siahsarani, Processing of AM60 magnesium alloy by hydrostatic cyclic expansion extrusion at elevated temperature as a new severe plastic deformation method, Int. J. Miner. Metall. Mater. 27 (2020) 669–677, https://doi.org/10.1007/s12613-019-1921-7.
[54] N. Nazemzadeh, A.A. Soufivand, N. Abolfathi, Computing the bond strength of 3D printed polylactic acid scaffolds in mode I and II using experimental tests, finite element method and cohesive zone modeling, Int. J. Adv. Manuf. Technol. 118 (2022) 2651–2667, https://doi.org/10.1007/s00170-021-08124-w.
[55] J.F. Peng, M.H. Zhu, Z.B. Cai, J.H. Liu, K.C. Zuo, C. Song, et al., On the damage mechanisms of bending fretting fatigue, Tribol. Int. 76 (2014) 133–141, https://doi.org/10.1016/j.triboint.2013.12.018.
[56] M.S.A. Parast, M. Azadi, Effect of nano-clay particles and heat treating on pure and fretting fatigue properties of piston aluminum alloy under stress-controlled cyclic bending loading, J. Mater. Eng. Perform. (2022) 1–16.
[57] J. Peng, B. Wang, X. Jin, Z. Xu, J. Liu, Z. Cai, et al., Effect of contact pressure on torsional fretting fatigue damage evolution of a 7075 aluminum alloy, Tribol. Int. 137 (2019) 1–10.
[58] J. Peng, J. Liu, Z. Cai, M. Shen, C. Song, M. Zhu, Study on bending fretting fatigue damages of 7075 aluminum alloy, Tribol. Int. 59 (2013) 38–46.
[59] Z. Huang, Z. Zhang, Z. Teng, M.K. Khan, Q. Wang, J. Wang, Effect of fretting damage on characteristics of high strength bearing steel up to very high cycle fatigue, Eng. Fract. Mech. 217 (2019) 106526.
[60] S. Mohd, Y. Mutoh, Y. Otsuka, Y. Miyashita, T. Koike, T. Suzuki, Scatter analysis of fatigue life and pore size data of die-cast AM60B magnesium alloy, Eng. Fail. Anal. 22 (2012) 64–72, https://doi.org/10.1016/j.engfailanal.2012.01.005.
[61] K. Yang, C. He, Q. Huang, Z.Y. Huang, C. Wang, Q. Wang, et al., Very high cycle fatigue behaviors of a turbine engine blade alloy at various stress ratios, Int. J. Fatig. 99 (2017) 35–43, https://doi.org/10.1016/j.ijfatigue.2016.11.032.
[62] J.F. Adams, J.E. Allison, J.W. Jones, The effects of heat treatment on very high cycle fatigue behavior in hot-rolled WE43 magnesium, Int. J. Fatig. 93 (2016) 372–386, https://doi.org/10.1016/j.ijfatigue.2016.05.033.
[63] K. Tokaji, M. Kamakura, Y. Ishiizumi, N. Hasegawa, Fatigue behaviour and fracture mechanism of a rolled AZ31 magnesium alloy, Int. J. Fatig. 26 (2004) 1217–1224, https://doi.org/10.1016/j.ijfatigue.2004.03.015.
[64] C. Potzies, K.U. Kainer, Fatigue of magnesium alloys, Adv. Eng. Mater. 6 (2004) 281–289.
[65] T.-S. Shih, W.-S. Liu, Y.-J. Chen, Fatigue of as-extruded AZ61A magnesium alloy, Mater. Sci. Eng., A 325 (2002) 152–162.
[66] Hashemi S. Abbaszadeh, K. Farhangdoost, W. Ma, D. Ghahremani Moghadam, R. Masoudi Nejad, F. Berto, Effects of tensile overload on fatigue crack growth in AM60 magnesium alloys, Theor. Appl. Fract. Mech. 122 (2022) 103573, https://doi.org/10.1016/j.tafmec.2022.103573.
[67] S. Fintová, L. Kunz, Fatigue properties of magnesium alloy AZ91 processed by severe plastic deformation, J. Mech. Behav. Biomed. Mater. 42 (2015) 219–228.
[68] D. Dimitrov, V. Shtarbakov, Ultrasonic fatigue test of AZ91 magnesium alloy, Mach Technol. Mater. 11 (2013) 50–53.

[69] S. Fintová, L. Trško, Z. Chlup, F. Pastorek, D. Kajánek, L. Kunz, Fatigue crack initiation change of cast AZ91 magnesium alloy from low to very high cycle fatigue region, Materials 14 (2021) 6245.
[70] S. Fintová, I. Kuběna, A. Chlupová, M. Jambor, I. Šulák, Z. Chlup, et al., Frequency-dependent fatigue damage in polycrystalline copper analyzed by FIB tomography, Acta Mater. 211 (2021) 116859.
[71] J. Polak, Cyclic Plasticity and Low Cycle Fatigue Life of Metals, Elsevier, Amsterdam, 1991.
[72] S.E. Stanzl-Tschegg, Influence of material properties and testing frequency on VHCF and HCF lives of polycrystalline copper, Int. J. Fatig. 105 (2017) 86–96.
[73] J. Peng, X. Jin, Z. Xu, J. Zhang, Z. Cai, Z. Luo, et al., Study on the damage evolution of torsional fretting fatigue in a 7075 aluminum alloy, Wear 402 (2018) 160–168.
[74] L. Nascimento, S. Yi, J. Bohlen, L. Fuskova, D. Letzig, K.U. Kainer, High cycle fatigue behaviour of magnesium alloys, Procedia Eng. 2 (2010) 743–750.
[75] Y. Song, H. Wang, B. Xu, Z. Xing, Effect of fretting wear on very high cycle bending fatigue behaviors of FV520B steel, Tribol. Int. 103 (2016) 132–138, https://doi.org/10.1016/j.triboint.2016.06.033.
[76] Z. Teng, H. Liu, Q. Wang, Z. Huang, P. Starke, Fretting behaviors of a steel up to very high cycle fatigue, Wear 438–439 (2019) 203078, https://doi.org/10.1016/j.wear.2019.203078.
[77] Z. Teng, H. Wu, Z. Huang, P. Starke, Effect of mean stress in very high cycle fretting fatigue of a bearing steel, Int. J. Fatig. 149 (2021) 106262, https://doi.org/10.1016/j.ijfatigue.2021.106262.
[78] G. Murugan, K. Raghukandan, U.T.S. Pillai, B.C. Pai, K. Mahadevan, High cyclic fatigue characteristics of gravity cast AZ91 magnesium alloy subjected to transverse load, Mater. Des. 30 (2009) 2636–2641.
[79] B. Ebel-Wolf, F. Walther, D. Eifler, Influence of elevated temperatures on the cyclic deformation behaviour of the magnesium die-cast alloys AZ91D and MRI 230D, Mater. Sci. Eng., A 486 (2008) 634–640.
[80] B. Wolf, C. Fleck, D. Eifler, Characterization of the fatigue behaviour of the magnesium alloy AZ91D by means of mechanical hysteresis and temperature measurements, Int. J. Fatig. 26 (2004) 1357–1363.
[81] M. Zolfaghari, M. Azadi, M. Azadi, Characterization of high-cycle bending fatigue behaviors for piston aluminum matrix SiO 2 nano-composites in comparison with aluminum–silicon alloys, Int. J. 15 (2021) 152–168.
[82] S.R. Shinde, D.W. Hoeppner, Fretting fatigue behavior in 7075-T6 aluminum alloy, Wear 261 (2006) 426–434.
[83] D. Du, D. Liu, X. Zhang, J. Tang, Fretting fatigue behaviors and surface integrity of Ag-TiN soft solid lubricating films on titanium alloy, Appl. Surf. Sci. 488 (2019) 269–276.
[84] C. Taltavull, B. Torres, A.J. López, J. Rams, Dry sliding wear behavior of AM60B magnesium alloy, Wear 301 (2013) 615–625, https://doi.org/10.1016/j.wear.2012.11.039.
[85] M. Mokhtarishirazabad, M. Azadi, G.H. Farrahi, G. Winter, W. Eichlseder, Improvement of high temperature fatigue lifetime in AZ91 magnesium alloy by heat treatment, Mater. Sci. Eng., A 588 (2013) 357–365.